Astron. Astrophys. 343, L61–L64 (1999)

ASTRONOMY AND ASTROPHYSICS

LETTER

Letter to the Editor

Forbidden lines from T Tauri disk winds

I. High magnetic torque models

S. Cabrit[1], **J. Ferreira**[2], **and A.C. Raga**[3]

[1] Observatoire de Paris, DEMIRM, URA 336 du CNRS, 61 Avenue de l'Observatoire, F-75014 Paris, France
[2] Laboratoire d'Astrophysique de l' Observatoire de Grenoble, B.P. 53, F-38041 Grenoble Cedex, France
[3] Instituto de Astronomía, UNAM, Ap. 70-264, 04510 D.F. México

Received 20 October 1998 / Accepted 3 February 1999

Abstract. We present synthetic emission maps and long-slit spectra in the [O I]6300 and [S II]6731 lines for self-similar, cold MHD disk winds of high magnetic torque. We find that such models produce both a dense, compact low-velocity component (LVC) and a lower density, collimated high-velocity component (HVC) sharing several observed properties of jets from T Tauri stars (resolved transverse sizes, strong apparent acceleration in [O I], larger spatial displacement and lower gradients in [S II]). Hence, the LVC and HVC observed in TTS might be formed in two distinct regions of the same wind. We suggest that disk wind models with lower ratio of magnetic to viscous torque and significant coronal heating at the wind base could compare even more favorably with the observations.

Key words: accretion, accretion disks – line: profiles – Magnetohydrodynamics (MHD) – stars: pre-main sequence – ISM: jets and outflows

1. Introduction

For over a decade, there has been mounting evidence that bipolar ejection from young stellar objects is powered by accretion and that magnetic fields play a crucial role in accelerating and collimating the wind (see e.g. Pudritz 1988; Cabrit et al. 1990). Yet, the exact launching mechanism remains to be identified. Ejection/accretion ratios $f \sim 0.01 - 0.1$ are inferred from observations of optical jets and molecular outflows (Hartigan et al. 1994; Hartigan, Edwards, & Gandhour 1995, hereafter HEG; Bontemps et al. 1996), but they could be accomodated by most proposed magneto-hydrodynamic (MHD) wind models. More specific constraints require detailed comparison of the observed and modelled wind structures, especially in regions very close to the star (< 150 AU) where jet instabilities and shocks with the ambient medium have (hopefully) not yet dramatically perturbed the flow. The velocity and density structure of these regions have become observable in T Tauri stars (TTS) thanks to spectro-imaging techniques (Solf 1997 and refs. therein; Hirth et al. 1994; Lavalley et al. 1997) and to narrow-band subarcsecond imaging (e.g. Ray et al. 1996). It is now crucial to provide theoretical predictions on comparable scales.

Shang et al. (1998) calculated images and long-slit spectra for a magnetic wind from the disk corotation radius ('X-wind'; cf. Shu et al. 1995) which reproduce several properties of the high-velocity component (HVC) of forbidden lines in TTS. An MHD wind from the disk surface has been proposed to explain the low-velocity component (LVC) of these lines (Kwan & Tademaru 1988,1995 [hereafter KT]; Hirth et al. 1994). As a further step in exploring observable diagnostics of disk winds in TTS, we present in this Letter calculations of forbidden line maps and long-slit spectra for the most complete MHD disk wind models available to date. Model characteristics are summarized in Sect. 2, synthetic maps and profiles are presented in Sect. 3, and implications are discussed in Sect. 4.

2. Self-similar magnetic accretion-ejection structures

2.1. Model hypotheses and parameters

Under the hypotheses that (1) a large scale bipolar magnetic field threads the accretion disk, (2) jet enthalpy is negligible, and (3) the structure is steady-state, axisymmetric, and self-similar with disk radius, Blandford & Payne (1982; hereafter BP) found the first solutions of self-collimated, super-alfvénic MHD disk winds. Safier (1993a,b) calculated the thermal equilibrium and total forbidden line profile of BP disk winds for TTS, and showed that they could readily account for the observed [S II] and [O I] fluxes in these stars. BP models, however, do not treat the inter-relation between the jet and the underlying disk. Thus, slow-point crossing is not constrained, leaving one extra degree of freedom in the solutions. Complete steady-state models of accretion-ejection structures further require to specify (4) a diffusion process in the disk allowing accreting matter to cross magnetic field lines: for the inner disk regions, one usually relies on a turbulent magnetic diffusivity (though ambipolar diffusion has also been used), and (5) a magnetic field

Send offprint requests to: sylvie.cabrit@obspm.fr

curvature in the disk, which determines the ratio Λ of magnetic torque to viscous torque. All models so far have high magnetic torques ($\Lambda \gg 1$). Wardle & Königl (1993) and Li (1995) obtained solutions by matching a magnetized disk to a BP jet, but used approximate equations to describe the disk vertical equilibrium. We will use here the more recent models of Ferreira (1997), which take into account all relevant dynamical terms through the slow-point (Ferreira & Pelletier 1995).

Three dimensionless parameters govern the self-similar accretion-ejection structure: (1) $\varepsilon = h/R$, where h is the disk scale height at the cylindrical radius R, (2) $\alpha_{\rm m} = \nu_{\rm m}/V_{\rm A}h$, where $\nu_{\rm m}$ is the required turbulent magnetic diffusivity and $V_{\rm A}$ the Alfvén velocity on the disk midplane, (3) $\xi = d\ln \dot{M}_{\rm acc}(R)/\, d\ln R$, the ejection efficiency parameter. Here, we have chosen $\varepsilon = 0.1$ (as estimated in HH 30 by Burrows et al. 1996) and $\alpha_{\rm m} = 1$. Solutions that extend far from the Alfvén surface are then found for ξ between 0.005 and 0.012 (see Ferreira 1997). In order to get physical values, we need to specify a central star mass M_*, which determines jet velocities through a keplerian scaling law, and a mass accretion rate $\dot{M}_{\rm acc}$, which then fixes the flow density. We take here $M_* = 0.7\,{\rm M}_\odot$ and $\dot{M}_{\rm acc} = 10^{-6}\,{\rm M}_\odot\,{\rm yr}^{-1}$, typical of TTS with strong jets (HEG). The solution is truncated at an inner radius $R_{\rm i}$ fixed here at the corotation radius: 0.07AU for an 8 day rotation period (within this radius, dynamics are likely to be dominated by magnetospheric — possibly wind-carrying — field lines). The ejection/accretion ratio is then $f \simeq \xi \ln(R_{\rm e}/R_{\rm i})$, where $R_{\rm e} \gg R_{\rm i}$ is the (unknown) outer radius of the MHD disk-wind.

2.2. Physical structure of the disk wind models

Fig. 1a illustrates the structure of the inner jet launching region for $\xi = 0.01$. Accreting matter located close to one disk scale-height is lifted up and flung out along a magnetic surface (we will denote $R_{\rm o}$ the radius of this field line footpoint). The wide opening of the streamlines causes a rapid drop off in density over a few scale heights, which globally results in an almost horizontal density stratification above the disk. This characteristic feature of self-similar disk-driven jets (e.g. Fig. 3 of Safier 1993a) arises because, at a given altitude above the disk plane, the drop-off has been more dramatic for the innermost regions than for the outer ones, and has roughly compensated for their initially higher mid-plane density ($\rho_{\rm o} \propto R_{\rm o}^{-1.5}$). The jet velocity is mostly rotational above the disk, until the vertical and radial components reach similar values at the Alfvén surface (located for this class of models at $Z \simeq R \simeq 10 \times R_{\rm o}$).

Beyond the Alfvén point, inertia overcomes magnetic tension and the magnetic field becomes more and more wrapped. The increasing hoop stress eventually recollimates the jet: when Z/R reaches a critical value $(Z/R)_{\rm c} \simeq 10$, streamlines reach a maximum cylindrical radius R_∞ and then very slowly refocus toward the axis. The expansion factor $R_\infty/R_{\rm o}$ increases from 50 to 2000 when ξ decreases from 0.01 to 0.005 (Ferreira 1997). Refocussing toward the jet axis is common to most MHD disk winds (although BP models used by Safier (1993a) recollimated only beyond 200 AU). As shown in Fig. 1b, there

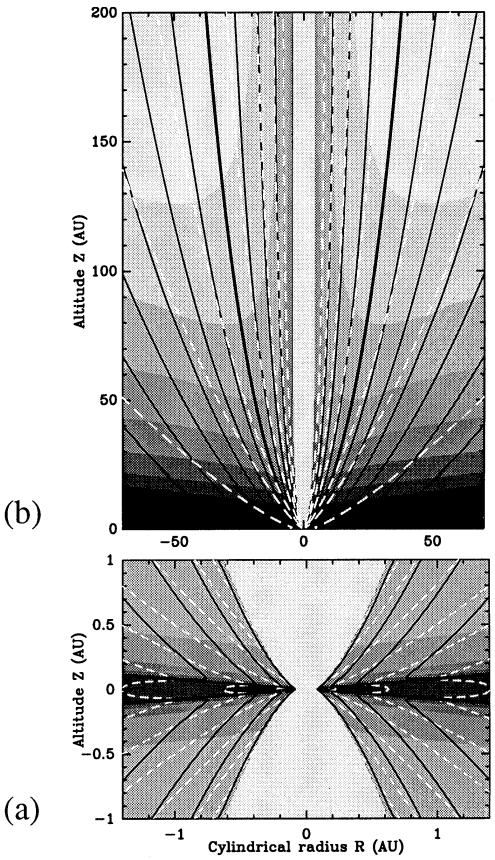

Fig. 1a and b. Cross-section of a self-similar accretion-ejection structure with ξ = 0.01 (other parameters in Sect. 2.1). Streamlines are drawn in black, contours of equal total velocity are drawn in white, and number density is shown in greyscale. **a** below the Alfvén surface; $\log_{10}(n_{\rm H}/{\rm cm}^{-3})$ greyscale from 7 to 12 by 1, velocity contours: 20, 30, 50, 100, 200 and 300 km/s. **b** beyond Alfvén surface. $\log_{10}(n_{\rm H})$ greyscale from 3.7 to 5.8 by 0.3, velocity contours: 10, 50, 100, 200, 300, 400, and 500 km/s. The $R_{\rm o} = 1$AU streamline is drawn in thick. Note the change in scale from **a** to **b**.

is a strong change in jet structure inside the recollimated region (a cone of opening angle $\theta = \arctan(Z/R)_{\rm c} \sim 6^o$). In this asymptotic regime, the jet velocity is mostly vertical for the solutions displayed here and, since most disk accretion power is finally converted into jet kinetic power ($\Lambda \gg 1$), its final value is $V_\infty(R_\infty) \simeq V_{\rm Kep}(R_{\rm o})\xi^{-1/2}$. Mass conservation then directly yields

$$\rho(R_\infty) \simeq \frac{\dot{M}_{\rm acc}\,\xi^{3/2}}{4\pi\sqrt{GM_*R_\infty^3}} \left(\frac{R_{\rm o}}{R_\infty}\right)^{1/2} \propto R_\infty^{-3/2} \times f(\xi).$$

Thus, inside the recollimation cone, density contours change from horizontal to vertical: Disk winds also produce the "optical illusion" described by Shu et al. (1995) for X-winds.

3. Synthetic emission maps and line profiles

We use the results of Safier (1993a) for the thermal equilibrium of BP disk winds heated by ambipolar diffusion: we assume that

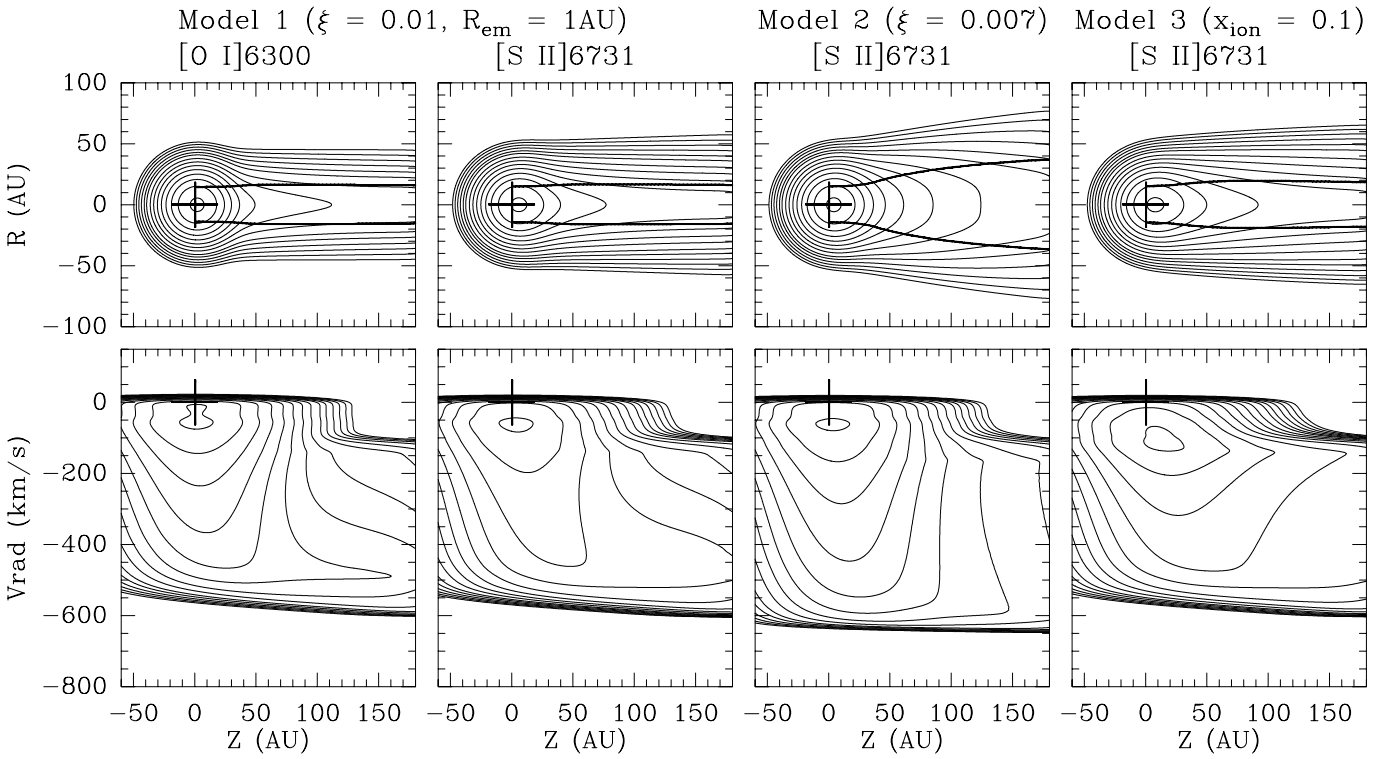

Fig. 2. *Top row:* emission maps convolved by a 28 AU beam (0.2" at 140 pc). Thick lines show the jet transverse FWHM as a function of position. *Bottom row:* long-slit spectra along the jet axis, convolved by 70 AU × 10 km/s (highest resolutions achieved so far in long-slit spectra of TTS). Contours increase by factors of 2. Map peak surface brightnesses are 0.12, 0.36, 0.18, 0.50 erg s^{-1} cm^{-2} sr^{-1} (*left* to *right*).

the flow is heated only above $Z/R \simeq 0.7$, and reaches a uniform electron temperature of 10^4 K and an ionization fraction $x_{\rm ion} = n_{\rm e}/n_{\rm H} \simeq 0.1\times$ (0.1 AU $/R_{\rm o}$). For $R_{\rm o} > R_{\rm em} \simeq 1$AU, the wind is assumed to remain mostly molecular and does not contribute any emission. We solve at each position the statistical equilibrium of the ground state multiplets of [O I] and [S II] assuming that oxygen ionization follows that of hydrogen, and that sulfur remains singly ionized throughout the flow. Elemental abundances are [O]/[H] = 6.6×10^{-4} and [S]/[H] = 1.6×10^{-5}. In Fig. 2 we present synthetic [O I]6300 and [S II]6731 maps and long-slit spectra for ξ = 0.01 and a view angle $i = 40^\circ$ from pole-on (Model 1); in additional panels we show the effect of a lower ξ = 0.007 (Model 2), and of a constant $x_{\rm ion} = 0.1$ (Model 3). The latter case might result e.g. if heating becomes dominated by internal shocks or instabilities.

3.1. Emission maps and jet transverse sizes

Maps are dominated by a strong unresolved peak at the origin, reflecting the steep drop in density above the disk plane. The intensity drops off faster in [O I]6300 than in [S II]6731, as [O I] has a 100 times higher critical density and is hence sooner in the low-density regime (intensity $\propto n_{\rm e}^2$). After convolution by our adopted PSF of 28 AU (HST-like resolution of 0.2" at the distance of Taurus), the emission peak is shifted out by ~ 3 AU in [O I]6300 and ~ 6 AU in [S II]. The shift would increase at lower angular resolution.

With a PSF of 28 AU, the jet transverse FWHM is found to depend very little on the chosen line tracer, ionization fraction distribution, flow density, inclination, or $R_{\rm em}$ value. It is mostly sensitive to the degree of opening of the innermost streamline, fixed by ξ: For ξ = 0.01, the FWHM stays constant at 30-40 AU (Models 1 and 3), while for ξ = 0.007 it increases steadily up to 80 AU at 180 AU from the star (Model 2).

3.2. Long-slit spectra

Synthetic long-slit spectra exhibit both a compact LVC and a spatially extended HVC. The LVC is formed in very dense regions just above the disk plane ($n_{\rm H} \sim 10^8$ cm^{-3}). There, the almost horizontal density stratification ensures that outer radii dominate (more volume). The LVC centroid is thus representative of the slow motions at $R_{\rm em}$, and a larger $R_{\rm em}$ would make the LVC narrower and less blueshifted. As shown by KT, the detailed shape of the LVC also depends strongly on the ratio of rotational to poloidal speed in the emitting region (here ~ 1 at $Z/R \sim 0.7$). The LVC is seen to be slightly more blueshifted and displaced from the star in [S II] than in [O I], a result of acceleration and expansion at the base of the disk wind (see Hirth et al. 1994; KT).

The HVC is formed further out in the wind. A range of velocity gradients is present: Inner streamlines accelerate over a short distance ($\simeq 10 - 20 R_{\rm i}$ for Models 1 and 2) to high velocities, while outermost streamlines accelerate over a large

distance to low asymptotic speeds. Since inner streamlines are denser, HVC acceleration will then *appear* stronger in a line of higher critical density. In Model 1 of Fig. 2, the [O I]6300 line is dominated by inner streamlines and therefore shows a steep velocity gradient. The [S II]6731 line, of lower critical density, shows a more moderate velocity gradient. With a lower ξ (Model 2), inner streamlines achieve cylindrical density collimation much later and are not yet dominant in spectra at $\simeq$ 100 AU of the star. When $x_{\rm ion}$ is kept constant (Model 3), the relative contribution of outer streamlines strongly increases and comes to dominate the [S II]6731 long-slit spectrum, in the form of a slowly accelerating component ($V_{\rm rad} \simeq$ -150 km/s).

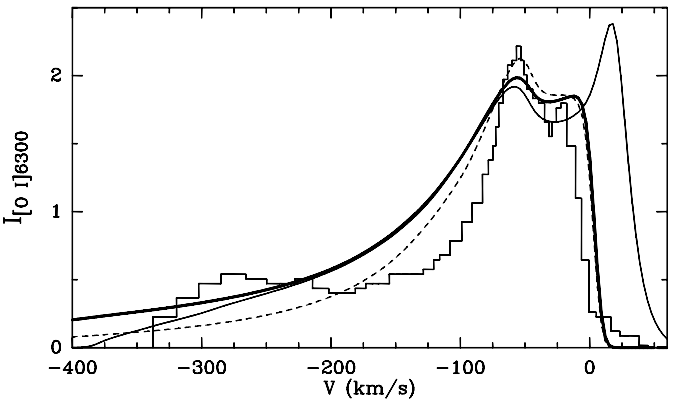

Fig. 3. [O I]6300 profile toward DG Tau (histogram; adapted from Solf [1997]) and synthetic profiles at the same spatial and spectral resolution (140 AU, 10 km/s): Thick line: Model 1 ($i = 40^\circ$); thin line: same model but $i = 60^\circ$; dashed line: constant $x_{\rm ion} = 0.1$ (Model 3).

4. Discussion

Even though our results are obtained for self-similar, cold, high magnetic torque ($\Lambda \gg 1$) MHD disk winds, they reveal several characteristic behaviors that should remain valid for more general cases of disk winds. The most striking result of our study is that disk winds produce not only a compact and dense LVC formed close to the disk surface (cf. KT) but also an extended, less dense, jet-like HVC. This HVC shares several observed properties of TTS jets: (1) The predicted jet FWHM of 30-80 AU at 28 AU resolution agree well with HST and adaptive optics measurements (Ray et al. 1996, Dougados et al. 1999); (2) The steep apparent acceleration in the high-velocity blue wing of [O I]6300, and larger spatial displacement and lower gradient in [S II]6731, are both commonly seen in TTS jets (e.g. Hirth et al. 1994; Solf 1997). In contrast, X-winds from the corotation region predict little difference between [O I] and [S II] long-slit spectra (Shang et al. 1998); (3) The relative intensity and velocity of the LVC and HVC agree well with the central line profile shape seen in e.g. the high accretion TTS DG Tau (Fig. 3), despite our crude assumptions about wind heating. Since LVC emission arises at densities above critical, while the HVC is mostly in the sub-critical regime, stars with lower accretion rates should have a lower HVC/LVC ratio in [O I]. This trend is indeed observed in TTS (HEG).

We anticipate that relaxing the assumptions of high magnetic torque ($\Lambda \gg 1$) and cold wind would produce even more favorable comparison with observations of TTS: In the high magnetic torque models investigated here, the terminal velocities of $\sim$ 10 times the initial keplerian speed (see Sect. 2.2) produce broad emission lines in the asymptotic jet region, while narrow lines are more frequently reported. A related property is that only a fraction $\sim \varepsilon$ of the available accretion power is radiated as infrared excess, while $\simeq$ 50% of it is radiated in the UV at the accretion shock or boundary layer. Such a difference between infrared and UV excess in TTS is not observed. MHD disk winds of smaller ratio of magnetic to viscous torque will help in providing both less extreme wind acceleration and larger viscous disk heating. Another improvement of current models would be to relax the assumption of a cold disk wind. Currently, the region heated by ambipolar diffusion extends only out to $R_{\rm em} \simeq$ a few AU and, as shown in Fig. 3, this would yield a double-peaked LVC at inclinations $i \geq 60^\circ$. The observation of a single-peaked LVC at most inclinations suggests that the disk wind surface is heated to $\sim 10^4$ K out to $\geq$ 10 AU (see KT). Since the sound speed then exceeds the local keplerian speed, the cold wind approximation must be relaxed to treat this situation. We conclude that disk winds with $\Lambda \lesssim 1$ and a hot corona at the base of the wind appear promising for explaining both the LVC and HVC of forbidden lines in TTS, and that self-consistent solutions including these ingredients should be investigated.

Acknowledgements. We are grateful to C. Dougados, S. Edwards, F. Gueth, H. Shang, F. Shu and the referee for helpful comments.

References

Blandford, R.D., Payne, D.G., 1982, MNRAS 199, 883 (BP)
Bontemps, S., André, P., Terebey, S., Cabrit, S. 1996, A&A 311, 858
Burrows, C.J. et al., 1996, ApJ 473, 437
Cabrit, S., Edwards, S., Strom, S., Strom, K.M. 1990, ApJ 354, 687
Dougados, C. et al., 1999, in preparation
Ferreira, J., Pelletier, G., 1995, A&A, 295, 807
Ferreira, J., 1997, A&A, 319, 340
Hartigan, P., Morse, J.A., Raymond, J. 1994, ApJ 436, 125
Hartigan, P., Edwards, S., Gandhour, L. 1995, ApJ 452, 736 (HEG)
Hirth, G., Mundt, R., Solf, J., 1994, A&A 285, 929
Kwan, J., Tademaru, E. 1988, ApJ 332, L41
Kwan, J., Tademaru, E. 1995, ApJ 454, 382 (KT)
Lavalley, C., Cabrit, S., Dougados, et al., 1997, A&A 327, 671
Li, Z.-Y., 1995, ApJ, 444, 848
Pudritz, R. 1988, in: Galactic and Extragalactic Star Formation, eds. R. Pudritz and M. Fich, Kluwer Academic Publishers, p.135
Ray, T.P., Mundt, R., Dyson, J.E., et al., 1996, ApJ 468, L103
Safier, P.N., 1993a, ApJ, 408, 115
Safier, P.N., 1993b, ApJ, 408, 148
Shang, H., Shu, F.H., Glassgold, A., 1998, ApJ, 493, L91
Shu, F.H., Najita, J., Ostriker, E., Shang, H., 1995, ApJ, 455, L155
Solf, J. 1997, Herbig-Haro Flows and the Birth of Stars; IAU Symposium No. 182, eds. B. Reipurth and C. Bertout. Kluwer Academic Publishers, p. 63-72
Wardle, M., Königl, A., 1993, ApJ, 410, 218